Biochem. J. (2003) **373**, 875–883 (Printed in Great Britain)

875

Structural and thermal stability analysis of *Escherichia coli* and *Alicyclobacillus acidocaldarius* thioredoxin revealed a molten globule-like state in thermal denaturation pathway of the proteins: an infrared spectroscopic study

Emilia PEDONE*, Simonetta BARTOLUCCI†[1], Mosè ROSSI†‡, Francesco Maria PIERFEDERICI§, Andrea SCIRÈ¶, Tiziana CACCIAMANI¶ and Fabio TANFANI¶

*Istituto di Biostrutture e Bioimmagini, C.N.R.,Via Mezzocannone 6, 80134, Napoli, Italy, †Dipartimento di Chimica Biologica, Università degli Studi di Napoli Federico II, via Mezzocannone 16, 80134 Napoli, Italy, ‡Istituto di Biochimica delle Proteine, via P. Castellino 111, 80131 Napoli Italy, §Dipartimento di Scienze Chimiche, Università degli Studi di Catania, viale A. Doria 6, 95125 Catania, Italy, and ¶Istituto di Biochimica, Università Politecnica delle Marche, via Ranieri, 60131 Ancona, Italy

The structure of thioredoxin from *Alicyclobacillus acidocaldarius* (previously named *Bacillus acidocaldarius*) (BacTrx) and from *Escherichia coli* (*E. coli* Trx) was studied by Fourier-transform IR spectroscopy. Two mutants of BacTrx [Lys^{18} → Gly (K18G) and Arg^{82} → Glu (R82E)] were also analysed. The data revealed similar secondary structures in all proteins, but BacTrx and its mutants showed a more compact structure than *E. coli* Trx. In BacTrx and its mutants, the compactness was p^{2}H-dependent. All proteins revealed the existence of a molten globule-like state. At p^{2}H 5.8, the temperature at which this state was detected was higher in BacTrx and decreased in the different proteins in the following order: BacTrx > R82E > K18G > *E. coli* Trx. At neutral or basic p^{2}H, the molten globule-like state was detected at the same temperature in both BacTrx and R82E, whereas it was found at the same temperature in all p^{2}Hs tested for *E. coli* Trx. The thermal stability of the proteins was in the following order at all p^{2}Hs tested: BacTrx > R82E > K18G > *E. coli* Trx, and was lower for each protein at p^{2}H 8.4 than at neutral or acidic p^{2}Hs. The formation of protein aggregates, brought about by thermal denaturation, were observed for BacTrx and K18G at all p^{2}Hs tested, whereas they were present in R82E and *E. coli* Trx samples only at p^{2}H 5.8. The results indicated that a single mutation might affect the structural properties of a protein, including its propensity to aggregate at high temperatures. The data also indicated a possible application of Fourier-transform IR spectroscopy for assessing molten globule-like states in small proteins.

Key words: Fourier-transform IR (FTIR) spectroscopy, molten globule-like state, protein aggregation, thermostability, thioredoxin, two-dimensional IR correlation analysis.

INTRODUCTION

Thioredoxin, a small (12 kDa) heat-stable protein found in all living cells from Archaea to humans, is a highly structured molecule with 90 % of its residues involved in secondary structural elements [1]. Thioredoxin has a central core of five β-sheet strands enclosed by four α-helices with the active-site disulphide bond (Cys^{32}–Cys^{35}) localized in a short loop at the N-terminus of the α2-helix. Thioredoxin plays a key role in various fundamental cellular processes [2], including deoxyribonucleotide biosynthesis, regulation of photosynthetic events, regeneration of oxidative damage and activation of transcription factors. Moreover, thioredoxin has been shown to be useful as a purification tag for the overexpression of economically valuable proteins and peptides [3,4]. The structural stability of thioredoxin from *Alicyclobacillus acidocaldarius* (BacTrx) has been shown to have higher thermostability when compared with the well-characterized thioredoxin from *Escherichia coli* (*E. coli* Trx) [5]. Studies investigating the simulation and structural comparison between the mesophilic and thermophilic protein revealed that one of the most important factors which increases the thermostability of BacTrx is given by the formation of new hydrogen-bond and salt-bridge interactions between side chains

[6,7]. Some of these interactions gave rise to hydrogen-bond networks that linked different secondary elements and increased the unfolding resistance. Simulation studies highlighted that Lys^{18} and Arg^{82} were especially interesting, because Lys^{18} Nζ acts as a hydrogen-bond donor with the Oδ1 Asp^{48} and Oε Gln^{105}, and the NH of the Arg^{82} side chain acts as a hydrogen-bond donor with CO Gln^{15}, CO Gly^{16} and Oδ1 Asp^{17} [6]. To remove electrostatic interactions, the two key residues Lys^{18} and Arg^{82} in BacTrx were replaced by the amino acids present in *E. coli* Trx, namely glycine and glutamic acid residues respectively [7]. The mutants were characterized by CD spectroscopy, spectrofluorimetry, thermodynamic comparative studies, limited proteolysis and molecular dynamic analysis at 500 K *in vacuo* [7]. The results were useful to evaluate the contribution of localized structural determinants of protein stability [7,8].

In the present study, the structure and thermal stability of *E. coli* Trx, BacTrx and Lys^{18} → Gly (K18G) and Arg^{82} → Glu (R82E) BacTrx mutants were characterized further. The experiments were performed at different pHs to evaluate the effect of defined salt bridges on the structural properties of the proteins. Fourier-transform IR (FTIR) spectroscopy was used in a first attempt to verify the presence of a molten globule-like state [9]. In fact, a study [10] using thermally denatured *E. coli* Trx in ^{1}H/^{2}H

---

exchange experiments combined with MS highlighted the existence of a collapsed unfolded state with properties often attributed to molten globule-like states, such as pronounced secondary structure combined with the absence of rigid tertiary structure, and thus a lack of protection against $^1H/^2H$ exchange. FTIR spectroscopy allowed us to show differences between *E. coli* Trx, BacTrx and its mutants, and to monitor protein conformational properties, including the presence of a molten globule-like state at definite temperatures in all proteins.

MATERIALS AND METHODS

Materials

Deuterium oxide (99.9 % ^2H_2O), ^2HCl and NaO^2H were purchased from Aldrich. All other chemicals were of the purest quality available.

Preparation and purification of thioredoxins

E. coli Trx, BacTrx and the K18G and R82E mutants of BacTrx were obtained and purified as described previously [5–7].

IR spectra

The proteins were analysed in three different buffers prepared in ^1H_2O or ^2H_2O at three different pHs or p^{2}Hs. The p^{2}H corresponds to the pH meter reading $+0.4$ [11]. The buffers used were: 50 mM Tris/HCl (or Tris/^{2}HCl), pH or p^{2}H 8.4 (buffer A); 50 mM Hepes/ NaOH (or Hepes/NaO^{2}H), pH or p^{2}H 7.0 (buffer B); and 50 mM piperazine/HCl (or piperazine/^{2}HCl), pH or p^{2}H 5.8 (buffer C). Typically, 1–1.5 mg of freeze-dried protein was dissolved in 200 μl of the appropriate buffer and concentrated into a volume of approx. 40 μl using a 10 kDa cut-off Centricon microconcentrator (Amicon) at 3000 ***g*** and 4 °C. A further 200 μl of buffer was added and the protein was concentrated again. This procedure was repeated several times in order to fully hydrate the protein with the chosen buffer. Sample preparation took 24 h, which is the contact time of the protein with ^2H_2O before spectra collection. The concentrated protein solution (approx. 35 μl) was then injected into a thermostat-controlled Graseby Specac 20500 cell (Graseby-Specac Ltd, Orpington, Kent, U.K.) fitted with CaF_2 windows and 6 or 25 μm spacers for measurements in ^1H_2O or ^2H_2O medium respectively. FTIR spectra were recorded at temperatures ranging from 20–99.0 °C, typically with 5 °C increments, and analysed as described previously [12]. The actual temperature in the cell was controlled by a thermocouple placed directly on to the window. Second derivative spectra were calculated over a five or nine data-point range (5 or 9 cm^{-1}). A five data-point range was used for spectra recorded at 20 °C in order to detect the amide I′ band components in more detail. It must be emphasized that, using the above-mentioned parameters, all peaks and shoulders detected in the resolution-enhanced spectra are real and not due to noise or water vapour absorption, as indicated by the absence of any small peaks in the 1750–1700 cm^{-1} region.

Generalized two-dimensional (2D) IR correlation analysis

Generalized 2D IR correlation analysis of IR band intensities of absorbance spectra in the 20.0–99.0 °C temperature range was performed as described by Noda [13]. To generate synchronous and asynchronous plots, 2Dcos toolbox software and Matlab 6.0 software (The MathWorks, Inc., Natick, MA, U.S.A.) were used.
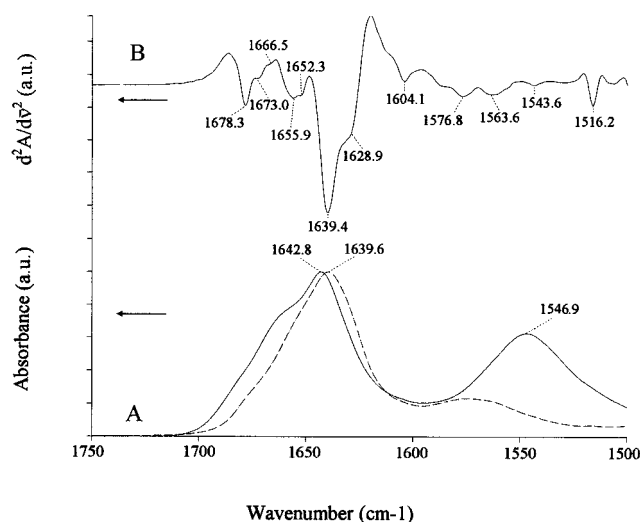

Figure 1   Absorbance (A) and second derivative (B) spectra of BacTrx at 20 °C

(**A**) Solid and broken lines refer to absorbance spectra of BacTrx in ^1H_2O at pH 8.4 and in ^2H_2O at p^{2}H 8.4 respectively. (**B**) Second derivative spectrum of BacTrx in ^2H_2O at p^{2}H 8.4. The spectrum was calculated over a five data-point range (5 cm^{-1}). The arrows indicate the *y*-axis label to which the spectra refer.

The 2Dcos toolbox software was developed in Professor Ozaki's laboratory (Kwansei Gakuin University, Sanda, Japan) by Berry and based on the paper [14]. The separation of IR spectra in different sets allows different events to be described in more detail [15] and thus, we considered three sets covering the 20.0–59.3 °C, 59.3–84.3 °C, and 84.3–99.0 °C temperature ranges. This separation allowed us to observe better the decrease in the 1628 cm^{-1} band intensity, the band-shift associated with $^1H/^2H$ exchange and denaturation/aggregation respectively. The analysis was done in the 1700–1600 cm^{-1} region for the spectra recorded in the 20.0–59.3 °C and 84.3–99.0 °C temperature ranges. In order to visualize the changes in the amide II band intensity, the spectra obtained in the 59.3–84.3 °C temperature range were analysed between 1700–1500 cm^{-1}.

RESULTS

Absorbance and second derivative spectra of BacTrx

Figure 1 shows the original absorbance spectrum of BacTrx at pH or p^{2}H 8.4. In ^1H_2O, the amide I and amide II bands showed maxima at 1642.8 and 1546.9 cm^{-1} respectively. In ^2H_2O, the amide I and amide II bands shifted to 1639.6 and 1446.4 cm^{-1} respectively (results not shown), as a consequence of the exchange of amide hydrogens with deuterium ($^1H/^2H$) [16]. In particular, the shift to lower wave numbers of the amide I′ is due to the shifts of its component bands (e.g. α-helix and β-sheet bands), and the higher the $^1H/^2H$ exchange in the secondary structural elements the higher the shift. The amide II band is particularly sensitive to the $^1H/^2H$ exchange and its shift to lower wave numbers caused a decrease in its intensity, which is a measure of the accessibility of the solvent (^2H_2O) to the protein. In our case, the large decrease in intensity of the amide II band indicates that the protein is largely accessible to the solvent.

In the amide I′ region, the second derivative spectrum revealed seven bands that, according to previous studies on proteins [17,18], may be assigned to particular secondary structures. The

1678.3, 1639.4 and 1628.9 cm^{-1} bands belong to a β-sheet, and this multiplicity reflects differences in hydrogen-bonding strength as well as differences in transition dipole coupling in different β-strands [19]. In particular, the latter band could be due to β-strands at the edge of a β-sheet (termed β-edge) that are not hydrogen-bonded to another polypeptide-extended chain, but to a different intra- or inter-molecular structure ([18] and references therein, and [20,21]). Indeed, it has been found [22] that there is an interaction between the fourth α-helix (residues 93–105) with two β-strands in both BacTrx and *E. coli* Trx, with the interaction being tighter in the former than in the latter. Moreover, it has been shown ([18] and references therein) that, in the α/β barrel structure, interactions established between the β-edge carbonyls and the α-helix side chains gave rise to an IR band close to 1625 cm^{-1}. For these reasons, in our opinion, the 1628.9 cm^{-1} band is probably due to intramolecular interactions between the β-edge and the fourth α-helix. It is not excluded, however, that the 1628.9 cm^{-1} band is also due to intermolecular interactions that in *E. coli* Trx were found to be pH-dependent [9]. Alternatively, the 1628.9 cm^{-1} band could be due to an unusually strongly hydrogen-bonded β-sheet or to β-structures interacting strongly with solvent [21]. The absorption of α-helices typically occurs between 1648–1656 cm^{-1} [18] and, thus, the 1655.9 and 1652.3 cm^{-1} bands could be associated with this secondary structure element. The presence of two bands probably reflects two populations of α-helices exposed differently to the solvent (^{2}H$_2$O). The association of the fourth α-helix (residues 93–105) with two β-strands [22] could have the effect of protecting this helix against ^{1}H/^{2}H exchange, with the consequence of absorption at higher wave numbers than α-helices more exposed to the solvent. The presence of turns was revealed unambiguously by the small peak close to 1666 cm^{-1}, whereas the 1673 cm^{-1} band may be due to turns and/or β-sheet [18,23]. The bands below 1620 cm^{-1} are due to amino acid side-chain absorption [24] and, in particular, the 1516.2 cm^{-1} band is due to tyrosine residues, whereas the 1576.8 and 1563.6 cm^{-1} bands are due to ionized carboxyl groups of aspartic and glutamic acid residues respectively. The 1543.6 cm^{-1} band is associated with residual amide I band absorption [16] and its low intensity indicates that a very low amount of amide hydrogens were not exchanged with deuterium during the preparation of the protein sample.

Secondary structure of K18G, R82E and *E. coli* Trx

Figure 2 compares the second derivative spectrum of BacTrx at p^{2}H 8.4 with those of K18G, R82E and *E. coli* Trx at the same p^{2}H. In the spectrum of *E. coli* Trx, the shoulder close to 1628 cm^{-1} was slightly visible and the band close to 1651 cm^{-1} was higher than in the control spectrum, suggesting that the interaction between the fourth α-helix and β-strands is very loose. Also, in the *E. coli* Trx spectrum, the main β-sheet band was found at 1637.6 cm^{-1}, indicating that the β-sheet structure is more accessible to the solvent in *E. coli* Trx than in BacTrx [16]. In the *E. coli* Trx spectrum, the higher intensity of the bands close to 1584 and 1515 cm^{-1} indicated that there is a higher content of aspartic acid and tyrosine residues in *E. coli* Trx than in BacTrx, which is consistent with the amino acid composition of the two proteins [6].

The spectrum of K18G displayed the main β-sheet band at 1637.6 cm^{-1}, as in the *E. coli* Trx spectrum, indicating that, in this protein, the β-sheet is more accessible to the solvent than in BacTrx. The slightly higher intensity of the band close to 1652 cm^{-1} and the slightly lower intensity of the band close to 1628 cm^{-1} suggested that in K18G the interaction between
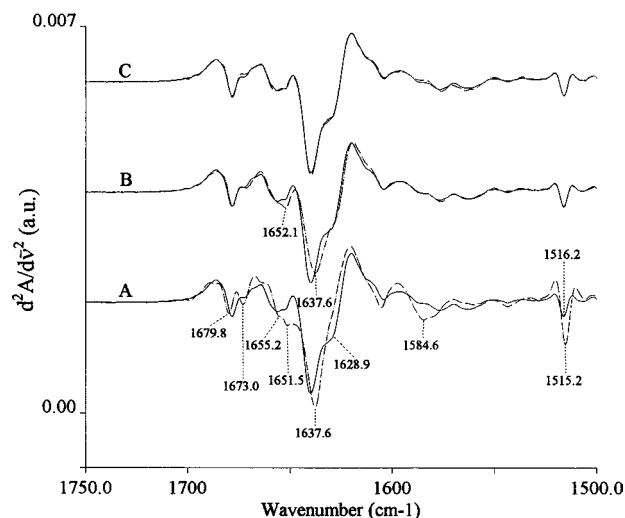

Figure 2   Second derivative spectra of BacTrx, K18G, R82E and *E. coli* Trx at 20 °C and p^{2}H 8.4

The broken lines represent the spectra of *E. coli* Trx (**A**), K18G (**B**) and R82E (**C**). The continuous line in (**A–C**) represents the spectrum of BacTrx (control). Second derivative spectra were calculated over a five data-point range (5 cm^{-1}).

the fourth α-helix and β-strands is less tight than in BacTrx. Similar results were obtained when comparing the BacTrx and K18G spectra at p^{2}H 7.0 and 5.8 (results not shown). No significant differences between the spectra of BacTrx and R82E were found at p^{2}H 8.4 (Figure 2) or at p^{2}H 7.0 and 5.8 (results not shown).

From these data and according to the position of the main β-sheet band, the accessibility of the solvent to the protein structure at 20 °C and p^{2}H 8.4 had the following order: *E. coli* Trx $\cong$ K18G > R82E $\cong$ BacTrx, whereas at p^{2}H 7.0 and 5.8 the order was: *E. coli* Trx > K18G > R82E $\cong$ BacTrx.

p^{2}H-induced conformational changes in BacTrx, K18G, R82E and *E. coli* Trx

Figure 3 shows the effect of p^{2}H on the secondary structure of BacTrx, K18G, R82E and *E. coli* Trx. Spectra of BacTrx (Figure 3A) showed that an increase in intensity and position of the main β-sheet band (1639.4 cm^{-1}) occurred with the decrease of p^{2}H. The band-shift to higher wave numbers indicated that, at p^{2}Hs lower than 8.4, the β-sheet became less accessible to the solvent. Figure 3(A) also shows that the decrease in p^{2}H induced an up-shift in wave number of the band close to 1678 cm^{-1}. Such parallelism with the shift of the band close to 1640 cm^{-1}, due to β-sheets, indicated that the band close to 1678 cm^{-1} was also due to β-sheets. Moreover, with the decrease in p^{2}H, the band close to 1629 cm^{-1} became more evident. This could be due to a strengthening of the hydrogen-bonded β-strand(s) involved in intramolecular interactions and/or as a consequence of the shift of the main β-sheet band to a higher wave number. The lowering of p^{2}H affects the structure of K18G (Figure 3B) and R82E (Figure 3C) mutants in a similar way, although for R82E the intensity and position of the main β-sheet band was less sensitive to p^{2}H changes. In the case of *E. coli* Trx (Figure 3D), the lowering of p^{2}H increased the intensity of the band close to 1655 cm^{-1}, indicating that the α-helices became less accessible to the solvent. Minor changes were observed at the level of the main β-sheet band.
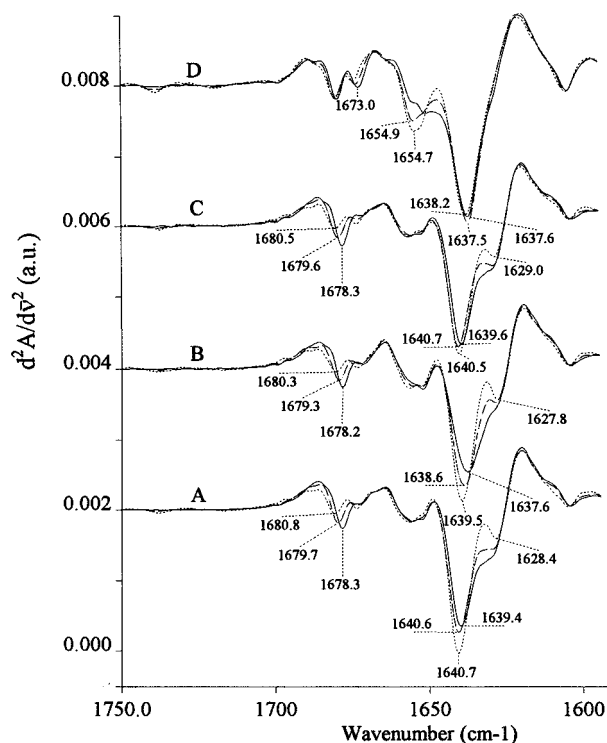
Figure 3 Effect of p²H on the second derivative spectra of BacTrx (A), K18G (B), R82E (C) and *E. coli* Trx (D) at 20 °C

The solid, broken and dotted lines refer to the spectra collected at p²H 8.4, 7.0 and 5.8 respectively. Second derivative spectra were calculated over a five data-point range (5 cm⁻¹).
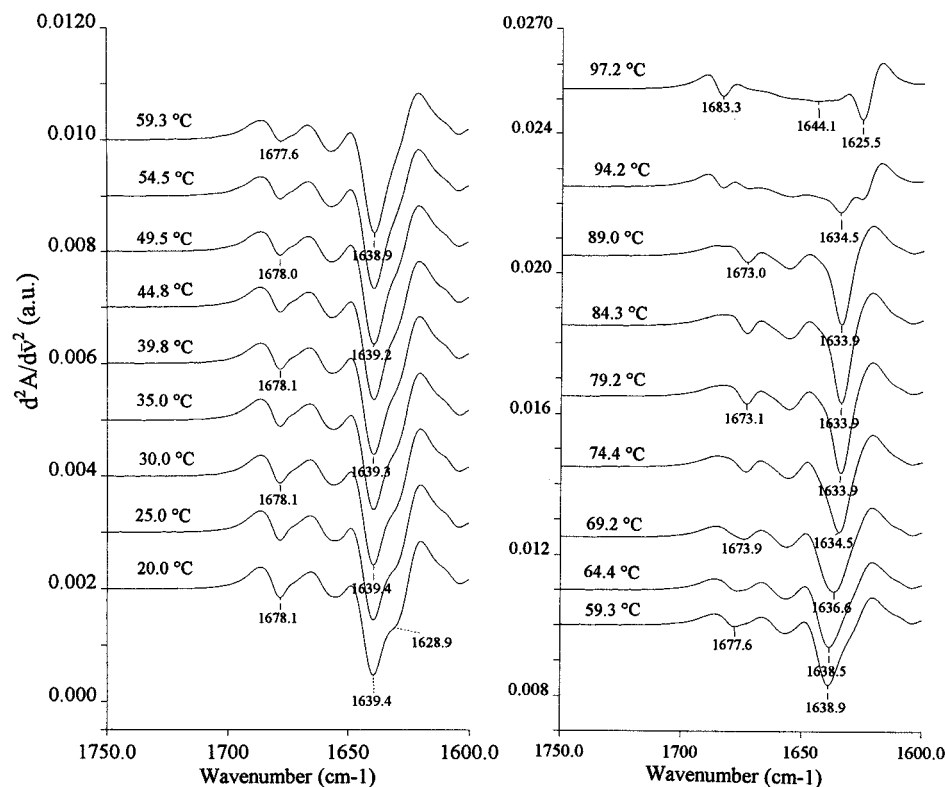
Thermal stability, protein aggregation and molten globule-like state

Figure 4 shows, as an example, the second derivative spectra of BacTrx at p²H 8.4 at different temperatures. Between 30.0 and 59.3 °C, the band close to 1628 cm⁻¹ decreased in intensity, suggesting the loosening of intramolecular hydrogen bonds involving the β-edge. Figure 4 also shows that a marked loss of secondary structural elements occurred at 94.2 and 97.2 °C, as indicated by the decrease in intensity or disappearance of the β-sheet and α-helix bands. No significant decrease in intensity of these bands occurred below 84.3 °C. The bands close to 1625 and 1683 cm⁻¹ seen at 94.2 and 97.2 °C indicated that, at these temperatures, the protein underwent aggregation (intermolecular interactions) brought about by thermal denaturation [25]. It is worth noting that protein aggregation occurred to a different extent in the different protein samples and this was found to be p²H-dependent, as shown in Table 1, which reports the intensity of the band close to 1625 cm⁻¹. In all cases, maximum protein aggregation occurred at acidic p²H, with *E. coli* Trx showing the lowest tendency to aggregate. At p²H 7.0 and 8.4, no aggregation bands were observed in the spectra of R82E and *E. coli* Trx. For K18G and BacTrx, aggregation occurred at all p²Hs tested, although at neutral p²H it appeared that this phenomenon arose to a lesser extent for both proteins. From these data, the formation of protein aggregates at high temperatures seems to be a complex phenomenon that may involve different protein and environmental parameters. In particular, at neutral or basic p²Hs a single point mutation (R82E) abolishes the formation of aggregates at high temperatures.

Figure 4 also shows that between 64.4 and 79.2 °C there was a marked downshift in wave number of the main β-sheet band,

Figure 4 Second derivative spectra of BacTrx at p²H 8.4 as a function of the temperature

Second derivative spectra were calculated over a nine data-point range (9 cm⁻¹). The actual temperature in the cell was controlled by a thermocouple placed directly on to the window.

Table 1 Formation of aggregates in BacTrx, R82E, K18G and *E. coli* Trx at high temperatures

The values (in absorbance units) refer to the intensity of the band close to 1625 cm^{-1} in the second derivative spectra of the proteins recorded at 97.2 °C multiplied by a factor of 10^4. *E. coli* Trx and the R82E mutant did not show significant aggregation bands at p^{2}H 7.0 and p^{2}H 8.4.

	Intensity of the aggregation band (absorbance units)			
p^{2}H	BacTrx	R82E	K18G	*E. coli* Trx
5.8	11.78	17.67	20.23	9.96
7.0	6.60	no	4.20	no
8.4	10.99	no	6.72	no
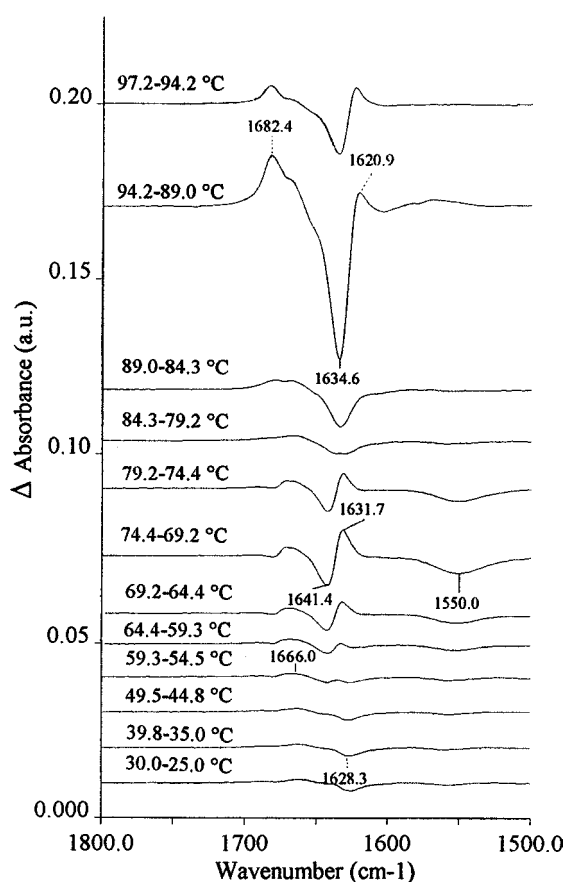
Figure 5 IR difference spectra of BacTrx at p^{2}H 8.4

Each trace was obtained by subtracting the original absorbance spectrum recorded at the lower temperature from the one recorded at the higher temperature (e.g. 94.2–89.0 °C). The actual temperature in the cell was controlled by a thermocouple placed directly on to the window.

which was also accompanied by a parallel shift of the band close to 1677 cm^{-1}. No decrease in band intensity was observed, indicating that, in this range of temperatures, there was no loss of secondary structure. The downshift in wave number of the main β-sheet band should be caused by a further ^{1}H/^{2}H exchange induced by a relaxation of the tertiary structure, since no changes in the secondary structure were detected.

In order to check this possibility, we calculated difference spectra, which allow the monitoring of even small changes between two absorbance spectra recorded at two different temperatures typically differing by 5 °C (Figure 5) [25]. Negative bands in the amide I$'$ region reflect protein denaturation [25] and/or band-shifts if positive adjacent bands of similar intensity are also present [12,26]. The latter case is applicable to the difference spectra in the range 64.4–79.2 °C. In fact, a negative band close to 1641 cm^{-1} and a positive one of similar intensity close to 1631 cm^{-1} were found within this temperature range, the most intense bands being detected in the 74.4–69.2 °C difference spectrum. Since the band close to 1641 cm^{-1} belongs to a β-sheet, its shift close to 1631 cm^{-1} indicated that the β-sheet became more exposed to the solvent (^{2}H$_2$O), thus allowing the protein to exchange residual amide hydrogens that were not exchanged during the preparation of protein sample. In fact, although the protein is largely accessible to the solvent, further ^{1}H/^{2}H exchange is supported by the appearance of the negative 1550 cm^{-1} peak (residual amide II band), which was seen in the difference spectra between 64.4–79.2 °C. In the difference spectrum 84.3–79.2 °C, the pair of negative and positive bands of similar intensity were not visible, indicating that no band-shifts take place within this range of temperatures. These data confirm those in Figure 4 and indicate that in the 64.4–79.2 °C temperature range the secondary structure does not change, whereas the tertiary structure undergoes relaxation with a consequent and further ^{1}H/^{2}H exchange. Thus this phenomenon describes a less-folded state in which the secondary structural elements are maintained and it may be associated with the presence of a molten globule-like state [27].

The other difference spectra confirm the data reported in Figure 4. In fact, at 89.0–84.3 °C, the protein starts to undergo significant denaturation, as revealed by the negative band close to 1634 cm^{-1}, and the maximum of denaturation was observed between 89.0 and 94.2 °C. In the 94.2–89.0 °C and 97.2–94.2 °C difference spectra, two positive bands close to 1620 and 1682 cm^{-1} reveal the formation of protein aggregation (intermolecular interactions) brought about by thermal denaturation [25]. The difference spectra between 59.3 and 30.0 °C showed a small negative band close to 1628 cm^{-1}, indicating that the intramolecular interactions involving the β-edge become looser. Moreover, a small and broad positive band at 1666 cm^{-1} indicates an increase in turn content induced by the increase of temperature.

Difference spectra (Figure 5), showing the details of events as a function of temperature, may be seen as a 'dynamic picture'. In order to test the information obtained by the difference spectra, we performed the generalized 2D IR correlation analysis [13]. This method allows synchronous and asynchronous spectra of dynamic spectral intensity variations induced by the increase in temperature to be obtained. A synchronous spectrum represents the simultaneous or coincidental changes of spectral intensities measured at two discrete and independent wave numbers ν_1 and ν_2 (on *x*- and *y*-axes respectively). An asynchronous spectrum represents sequential or unsynchronized changes of spectral intensities measured at ν_1 and ν_2 [13]. Autopeaks are present only on the diagonal of a synchronous map. Cross peaks are present in either synchronous or asynchronous maps at the off-diagonal positions and they can be positive or negative. The sign of synchronous cross peaks becomes positive if the spectral intensities at corresponding wave numbers are either increasing or decreasing together as a function of temperature. Negative synchronous cross peaks indicate that one of the spectral intensities is increasing while the other is decreasing. The sign of asynchronous cross peaks becomes positive if the intensity change at ν_1 occurs predominantly before ν_2. On the other hand, it becomes negative if the change occurs after ν_2. This rule is reversed if the synchronous cross peak at ν_1 and ν_2 is negative [13,28].

Figure 6 shows the synchronous (Figures 6A, 6C and 6E) and asynchronous (Figures 6B, 6D and 6F) spectra for BacTrx at p^{2}H

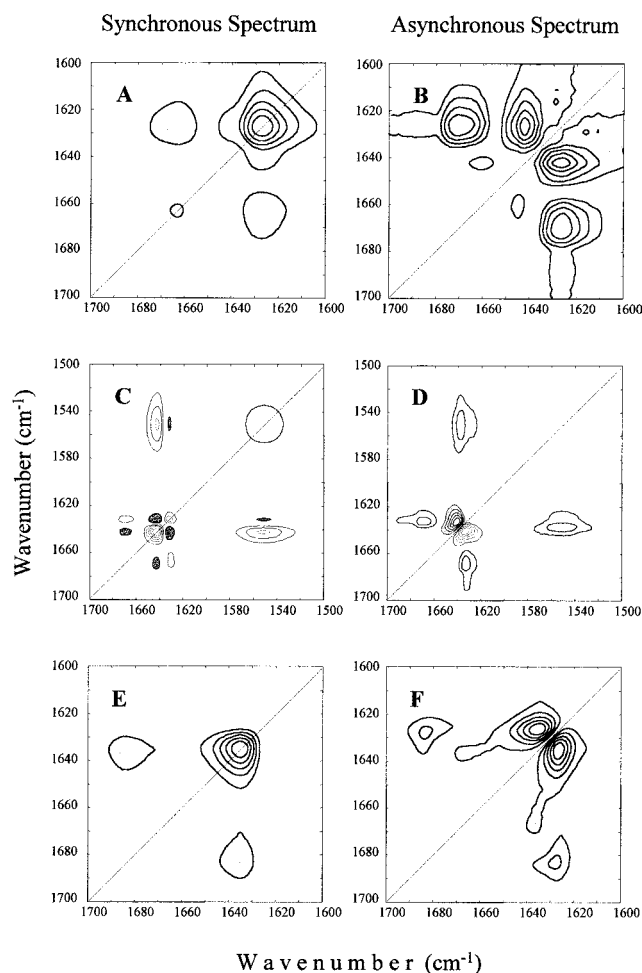Synchronous Spectrum   Asynchronous Spectrum

Figure 6   2D IR correlation analysis for the original absorbance spectra of BacTrx at p²H 8.4

The IR spectra in the 20–59.3 °C (**A** and **B**), 59.3–84.3 °C (**C** and **D**) and 84.3–99.0 °C (**E** and **F**) temperature ranges were subjected to 2D IR correlation analysis. Synchronous (**A**, **C** and **E**) and asynchronous (**B**, **D** and **F**) spectra are shown. Positive and negative peaks are represented in white and grey respectively. Multiple lines represent intense peaks.

8.4. Following the above-mentioned rules, Table 2 summarizes the information contained in Figure 6. The relative changes in band intensities at two independent wave numbers, obtained from synchronous plots in the three sets of temperature ranges, were in agreement with the second derivative and difference spectra. In particular, in the 59.3–84.3 °C range (Figure 6C), the autopeaks at 1551, 1632 and 1641 cm⁻¹ and the cross peaks (1641, 1551), (1641, 1632) and (1632, 1551) cm⁻¹ are correlated. In fact, difference spectra showed that, as a consequence of ¹H/²H exchange, the intensity of the bands at 1641 and 1550 cm⁻¹ decreased, whereas the intensity of the 1632 cm⁻¹ band increased. Small differences appeared when comparing the sequence of events obtained from asynchronous maps with second derivative and/or difference spectra. The differences involved the bands close to 1640 and 1684 cm⁻¹. These bands have been marked with an asterisk (*) in Table 2. In particular, 2D IR correlation analysis indicated that, in the 20–59.3 °C temperature range, changes in intensity of two small 1666 and 1642 cm⁻¹ bands preceded the decrease in intensity of the 1628 cm⁻¹ band which is the main event. Although the 1666 cm⁻¹ band was visible in the difference spectra, the 1642 cm⁻¹ band was not detected (at least in the unexpanded spectra). This small band may be due to loops/β-sheets/unordered structures. In the 59.3–84.3 °C range, the asynchronous map indicated that the decrease in intensity of the 1641 cm⁻¹ band occurred predominantly before the changes in intensity of the 1551 and 1632 cm⁻¹ bands. This result from the theoretical point of view is not consistent with the effect induced by further ¹H/²H exchange, since the changes in intensity of the 1641, 1551 and 1632 cm⁻¹ band should occur concomitantly as described for difference spectra (Figure 5). Indeed, 2D IR correlation analysis indicated that the latter two bands concomitantly changed their intensities. Hence the discrepancy concerning the 1641 cm⁻¹ band may be related to the fact that this peak, besides β-sheet, contains information related to other secondary structural elements. A similar hypothesis concerns the 1684 cm⁻¹ band in the 84.3–99.0 °C range. In fact, the asynchronous plot indicated that the intensity increase of this band occurred after the increase in intensity of the 1625 cm⁻¹ peak. This result is not consistent with the fact that new bands close to 1620 and 1680 cm⁻¹, being characteristic of intermolecular interactions brought about denaturation, always increase in intensity concomitantly. Hence it is likely that

Table 2   Correlation table for the original absorbance spectra of BacTrx at p²H 8.4

IR spectra were analysed separately in the 20–59.3 °C, 59.3–84.3 °C and 84.3–99.0 °C temperature ranges respectively. The data for the temperature ranges are taken from Figure 6 as follows: 20–59.3 °C (Figures 6A and 6B), 59.3–84.3 °C (Figures 6C and 6D) and 84.3–99.0 °C (Figures 6E and 6F). The two values reported in brackets, and concerning either synchronous or asynchronous spectra, describe a cross peak represented by two discrete and independent wave numbers (ν_1, ν_2) (on x- and y-axes respectively). The sign + or − after the brackets indicates a positive or negative cross peak. ↑ and ↓ indicate the increase and decrease respectively, in the intensity of the band at ν_1 or ν_2. (*) See text.

| Temperature ranges (°C)	Synchronous spectrum		Asynchronous spectrum	
	Auto peaks (cm⁻¹)	Cross peaks at x, y (cm⁻¹)	Cross peaks at x, y (cm⁻¹)	Sequence of events for individual components
20.0–59.3	1627, 1665	(1665↑, 1627↓)−	(1666, 1627)−, (1642, 1627)+, (1663, 1642)+	1666↑ turns *1642↓ loops/β-sheet/others 1628↓ β-edge
59.3–84.3	1550, 1632, 1641	(1641↓, 1551↓)+, (1641↓, 1632↑)−, (1666↑, 1632↑)+, (1666↑, 1641↓)−, (1632↑, 1551↓)−	(1641, 1551)+, (1641, 1632)−, (1666, 1632)+	1666↑ turns *1641↓ β-sheet /others 1551↓, 1632↑ ¹H/²H exchange
84.3–99.0	1635	(1684↑, 1635↓)−	(1635, 1625)+, (1684, 1625)−	1635↓ denaturation 1625↑ aggregation *1684↑ aggregation/turns/unknown
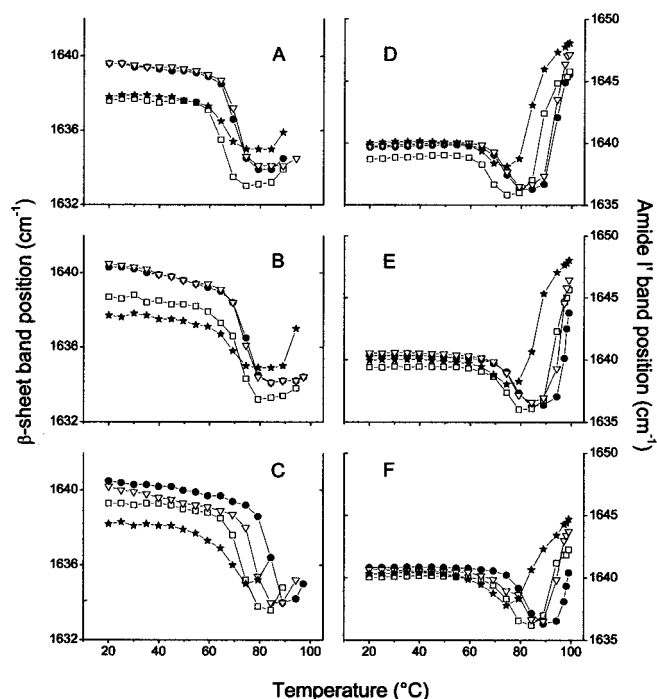
Figure 7   Temperature-dependent position of the main β-sheet band in the second derivative spectra of (A–C) and thermal denaturation curves for (D–F) BacTrx, R82E, K18G and *E. coli* Trx

The data were obtained at p²H 8.4 (**A** and **D**), 7.0 (**B** and **E**) and 5.8 (**C** and **F**) respectively. ●, BacTrx; ▽, R82E; □, K18G; and ★, *E. coli* Trx.

the 1684 cm⁻¹ band contains information on other secondary structural elements, including turns. Apart from the small discrepancies concerning the mentioned bands, 2D IR correlation analysis was consistent with the events shown by difference spectra.

The molten globule-like state was found in the thermal denaturation pattern of all proteins at all p²Hs tested (results not shown), and it may be described by a downshift in wave number of the main β-sheet band without any loss in the secondary structure. The temperature-dependent position of the main β-sheet band for all proteins at different p²Hs is shown in Figures 7 (A–C), and the characteristics of each curve are summarized in Table 3.

The temperature at which the maximum band-shift (MBS) occurred decreased with the increase in the p²H for all proteins with the exception of *E. coli* Trx, which showed almost the same MBS value at the different p²Hs tested. At p²H 5.8, the MBS value had the following order: BacTrx > R82E > K18G > *E. coli* Trx; at p²H 7.0 the order was: BacTrx = R82E > K18G > *E. coli* Trx; and at p²H 8.4 the order was: BacTrx = R82E > K18G = *E. coli* Trx. These data indicate that the point mutations affect the temperature of the formation of the molten globule-like state to a larger extent at acidic than at neutral or basic p²Hs, and this is particularly true for the R82E mutant, since it shows the same MBS values of BacTrx at p²H 7.0 and 8.4.

Figures 7 (D–F) shows the thermal denaturation curves obtained by monitoring the position of the amide I′ band as a function of the temperature [12]. At all p²Hs tested, the proteins display two transitions, the first indicated by a decrease and the second by a steady increase in the amide I′ band maximum. The same results were also obtained by monitoring other parameters of the IR spectrum such as the amide I′ bandwidth (results not shown).

Table 3   Temperature ranges of downshift in wave number of the main β-sheet band for BacTrx, R82E, K18G and *E. coli* Trx at different p²Hs

The temperature of the maximum β-sheet band-shift was obtained by calculating the inflection point of the curves reported in Figures 7 (A–C).

(a)

p²H	Temperature range of β-sheet band-shift (°C)			
	BacTrx	R82E	K18G	*E. coli* Trx
5.8	75.0–90.0	70.0–85.0	65.0–85.0	55.0–70.0
7.0	65.0–85.0	65.0–85.0	60.0–80.0	60.0–75.0
8.4	65.0–80.0	65.0–80.0	60.0–75.0	60.0–75.0

(b)

p²H	Temperature of maximum β-sheet band-shift (°C)			
	BacTrx	R82E	K18G	*E. coli* Trx
5.8	84.3	76.5	72.8	64.9
7.0	74.4	74.4	71.8	65.8
8.4	71.3	71.3	65.7	65.8

Table 4   Parameters of thermal denaturation curves for BacTrx, R82E, K18G and *E. coli* Trx at different p²Hs

(a)

p²H	Temperature range of first transition (°C)			
	BacTrx	R82E	K18G	*E. coli* Trx
5.8	70.0–90.0	65.0–90.0	65.0–85.0	55.0–75.0
7.0	65.0–85.0	65.0–85.0	65.0–80.0	65.0–75.0
8.4	65.0–80.0	65.0–80.0	60.0–75.0	60.0–75.0

(b)

p²H	Onset of second transition (°C)			
	BacTrx	R82E	K18G	*E. coli* Trx
5.8	94.2	89.0	89.0	79.2
7.0	94.2	89.0	89.0	79.2
8.4	89.0	84.3	79.2	79.2

(c)

p²H	T_m (°C)			
	BacTrx	R82E	K18G	*E. coli* Trx
5.8	97.3	94.3	93.0	89.0
7.0	97.2	95.0	93.0	86.9
8.4	94.0	93.0	88.5	84.3

Table 4 summarizes the features of the curves for all proteins tested. The first and second transition of the curves reflected the presence of a molten globule-like state and protein denaturation respectively. At all p²Hs, the thermal stability of the proteins, as indicated by their melting temperature (T_m), was: BacTrx > R82E > K18G > *E. coli* Trx. When comparing the same protein at different p²Hs, it appeared that, at p²H 5.8 or 7.0, BacTrx, R82E and K18G have the same or very similar T_m, whereas the stability of these proteins decreased significantly at basic p²H. Conversely, the stability of *E. coli* Trx was more sensitive to p²H, since it decreased continuously from p²H 5.8 to p²H 8.4.

DISCUSSION

Secondary structure

IR analysis of proteins revealed a similar secondary structure composition in BacTrx and its mutants, as well as in *E. coli* Trx. The spectra were characterized by a main β-sheet band and a parent band close to 1678 cm^{-1}, a distinguishing feature of an anti-parallel β-sheet conformation [18], which is consistent with the so-called thioredoxin motif [1,29]. The assignment of the 1628 cm^{-1} band to β-strands involved in intramolecular interactions was less straightforward, but is supported by the literature [18,22]. Intermolecular interactions also could contribute to this band, since in a previous calorimetric study [9] it was shown that, in the pH range 6–8, oxidized *E. coli* Trx undergoes dimerization, especially at low pH. It must be pointed out, however, that protein oligomerization is strongly influenced by sample concentration, which is different for calorimetric and FTIR spectroscopic measurements. In the case of an incorrect interpretation of the 1628 cm^{-1} band, this will not influence the main results concerning the molten globule-like state, since it has been detected analysing the characteristics of the bands close to 1638 cm^{-1} and 1550 cm^{-1}, which are recognized to be due to β-sheets and residual amide II band respectively. The NMR solution structure of BacTrx also showed that residues 57–59 might be involved in a 3_{10} helix or turns [19]. IR spectra, however, did not detect any significant peaks that could be attributed specifically to this secondary structural element, probably because of its very low content or as 3_{10} helix absorbs between 1662–1666 cm^{-1}, where turns typically absorb [30].

Packing

The FTIR data presented in this study have shown that, although to a differing extent, lowering of p^{2}H induces a more compact structure in all proteins and that BacTrx is more compact than *E. coli* Trx at all the p^{2}Hs tested, findings in agreement with NMR [22] and quartz nanogravimetric [5] data. The higher compactness at acidic, rather than at neutral or basic, p^{2}H may be associated with the changes involving ionic interactions. Point mutations altering ionic interactions and/or hydrogen bonds also affected the BacTrx compactness, but not always. K18G led to the loosening of the structure of BacTrx, whereas R82E had no relevant effect on the secondary or tertiary structure of the protein. Amino acid substitutions was done at the level of the first (K18G) and fourth (R82E) turns, and the destabilizing effect of K18G derives from the substitution of the positive charged Lys[18], whose side chain is involved in electrostatic interaction with Asp[48] and/or Asp[17]. On the other hand, the lack of the hydrogen bond between Arg[82] and Pro[83] in R82E [22] does not appear very important for protein compactness.

Thermal stability and protein aggregation at high temperatures

When comparing the T_m values of different proteins at the same p^{2}H, protein thermostability seems to parallel its compactness. In all cases, the single mutation lowered the thermal stability of the protein, with K18G being the most effective. The high number of ionic interactions in BacTrx is most probably the main factor in enhancing its thermostability. In fact, the almost identical number of hydrogen bonds present in BacTrx and *E. coli* Trx [22] suggests that they are not responsible for the markedly different thermostability of the proteins.

Protein aggregation (intermolecular interactions) can occur as a consequence of different phenomena, including protein misfolding [31], and thermal- [25] and/or organic solvent-induced denaturation [21,32]. In the present study, the data on protein aggregation (intermolecular interactions), brought about by protein denaturation at high temperatures, indicate that this phenomenon is sensitive to p^{2}H and even to a single mutation. The R82E mutant abolished aggregation at p^{2}H 7.0 and 8.4, whereas the K18G mutant retained the propensity of BacTrx to aggregate and, at acidic p^{2}H, this propensity was even higher than the control. Due to the complexity of the protein aggregation phenomenon, it is difficult to explain these results and one may observe that it seems to occur to a lower extent at neutral p^{2}H. The tendency of many proteins to aggregate at high temperatures was observed in many, but not all, instances, thus indicating further the complexity of the phenomenon.

Molten globule-like state

Partly unfolded states of proteins include the molten globule that has been observed for a number of proteins under different conditions, including at low pH and/or high temperatures, at moderately low dielectric constant [33] and in the presence of denaturants. The molten globule is more expanded compared with the native state of proteins and possesses the native-like secondary structure. The relaxation of tertiary structure and the existence of water inside the globule has been demonstrated by NMR ([34] and references therein) and deuterium exchange [35,36]. The peculiar characteristics of the molten globule fit with our observation of a further ^{1}H/^{2}H exchange and with the lack of significant changes in the secondary structure of the proteins observed within the temperature range corresponding to the first transition in the thermal denaturation curves. Our present data are also supported by the observation [10] that *E. coli* Trx in 2% acetic acid revealed the presence of a collapsed unfolded state with properties attributed to molten globule-like states, such as pronounced secondary structure and absence of a rigid tertiary structure. In one instance (K18G), the point mutation lowered the temperature of molten globule formation at all p^{2}Hs, whereas, for R82E, this phenomenon was only observed at acidic p^{2}H (Table 3). Also, considering BacTrx and its mutants, the changes in p^{2}H induced a different temperature of molten globule formation in each protein. In the case of *E. coli* Trx, the temperature of molten globule formation changes slightly when the p^{2}H is raised from 5.8–7.0 or 8.4. Hence even a single mutation and/or the variation of pH may influence the temperature of molten globule formation. It is likely that the point mutation or the changes of p^{2}H disrupt or loose ionic interactions and/or hydrogen bonds that stabilize the tertiary structure of the proteins.

It is worth emphasizing that the description of a molten globule-like state in a β-sheet-rich protein by FTIR spectroscopy was followed by monitoring the position of the amide I' band and analysing the ^{1}H/^{2}H exchange, the position and intensity of the main β-sheet band as a function of the temperature. Indeed, IR spectroscopy shows a higher sensitivity in detecting β-sheet than α-helices. In the case of a protein with a low content of β-sheets, the detection of a molten globule state is probably much more difficult or not possible. Moreover, we analysed the structure of a small protein. In the case of a bigger protein, even with a high content of β-sheets but with different domains, it would be very difficult to unambiguously assign changes in the characteristics of a β-sheet band to the formation of a molten globule-like state. In a previous study [12], it was suggested that the porcine odorant-binding protein, characterized by a β-barrel structure and a molecular mass of 20 kDa, forms a molten globule-like state. This suggestion arose as a result of IR data similar to those

reported in the present study but, in that case, there were no reports demonstrating the presence of a molten globule-like state by other techniques. In the case of thioredoxin, IR data are supported by NMR studies [10] and, hence, the results in the present paper may indicate a possible application of FTIR spectroscopy for assessing molten globule-like states in small β-sheet-rich proteins.

REFERENCES

1 Eklund, H., Gleason, F. K. and Holmgren, A. (1991) Structural and functional relations among thioredoxins of different species. Proteins: Struct., Funct., Genet. **11**, 13–28

2 Buchanan, B. B., Schurmann, P., Decottignies, P. and Lozano, R. M. (1994) Thioredoxin: a multifunctional regulatory protein with a bright future in technology and medicine. Arch Biochem. Biophys. **314**, 257–260

3 LaVallie, E. R., Di Blasio, E. A., Kovacic, S., Grant, K. L., Schendel, P. F. and McCoy, J. M. (1993) A thioredoxin gene fusion expression system that circumvents inclusion body formation in the *E. coli* cytoplasm. Bio/Technology **11**, 187–193

4 Yasukawa, T., Kanei-Ishii, C., Maekawa, T., Fujimoto, J., Yamamoto, T. and Ishii, S. (1995) Increase of solubility of foreign proteins in *Escherichia coli* by coproduction of the bacterial thioredoxin. J. Biol. Chem. **270**, 25328–25331

5 Bartolucci, S., Guagliardi, A., Pedone, E., De Pascale, D., Cannio, R., Camardella, L., Rossi, M., Nicastro, G., de Chiara, C., Facci, P. et al. (1997) Thioredoxin from *Bacillus acidocaldarius*: characterization, high-level expression in *Escherichia coli* and molecular modelling. Biochem. J. **328**, 277–285

6 Pedone, E., Bartolucci, S., Rossi, M. and Saviano, M. (1998) Computational analysis of the thermal stability in thioredoxins: a molecular dynamics approach. J. Biomol. Struct. Dyn. **16**, 437–446

7 Pedone, E., Cannio, R., Saviano, M. Rossi, M. and Bartolucci, S. (1999) Prediction and experimental testing of *Bacillus acidocaldarius* thioredoxin stability. Biochem. J. **15**, 309–317

8 Pedone, E., Saviano, M., Rossi, M. and Bartolucci, S. (2001) A single point mutation (Glu85Arg) increases the stability of the thioredoxin from *Escherichia coli*. Protein Eng. **14**, 255–260

9 Ladbury, J. E., Wynn, R., Homme, W., Hellinga, H. W., Julian, M. and Sturtevant, J. M. (1993) Stability of oxidized *Escherichia coli* thioredoxin and its dependence on protonation of the aspartic acid residue in the 26 position. Biochemistry **32**, 7526–7530

10 Maier, C. S., Schimerlik, M. I. and Deinzer, M. L. (1999) Thermal denaturation of *Escherichia coli* thioredoxin studied by hydrogen/deuterium exchange and electrospray ionization mass spectrometry: monitoring a two-state protein unfolding transition. Biochemistry **38**, 1136–1143

11 Salomaa, P., Schaleger, L. L. and Long, F. A. (1964) Solvent deuterium isotope effects on acid–base equilibria. J. Am. Chem. Soc. **86**, 1–7

12 Paolini, S., Tanfani, F., Fini, C., Bertoli, E. and Pelosi, P. (1999) Porcine odorant-binding protein: structural stability and ligand affinities measured by Fourier transform infrared spectroscopy and fluorescence spectroscopy. Biochim. Biophys. Acta **1431**, 179–188

13 Noda, I. (1993) Generalized two-dimensional correlation method applicable to infrared, raman and other types of spectroscopy. Appl. Spectrosc. **47**, 1329–1336

14 Sasic, S., Muszynski, A. and Ozaki, Y. (2000) A new possibility of the generalized two-dimensional correlation spectroscopy. 1. sample–sample correlation spectroscopy. J. Phys. Chem. A **104**, 6380–6387

15 Fabian, H., Mantsch, H. H. and Schultz, C. P. (1999) Two-dimensional IR correlation spectroscopy: Sequential events in the unfolding process of the λ Cro-V55C repressor protein. Proc. Natl. Acad. Sci. U.S.A. **96**, 13153–13158

16 Osborne, H. B. and Nabedryk-Viala, E. (1982) Infrared measurements of peptide hydrogen exchange in rhodopsin. Methods Enzymol. **88**, 676–680

17 Byler, D. M. and Susi, H. (1986). Examination of the secondary structure of proteins by deconvolved FTIR spectra. Biopolymers **25**, 469–487

18 Arrondo, J. L. R., Muga, A., Castresana, J. and Goñi, F. M. (1993) Quantitative studies of the structure of proteins in solutions by Fourier-transform infrared spectroscopy. Prog. Biophys. Mol. Biol. **59**, 23–56

19 Surewicz, W. K., Mantsch, H. H. and Chapman, D. (1993) Determination of protein secondary structure by Fourier transform infrared spectroscopy: a critical assessment. Biochemistry **32**, 389–394

20 Casal, H. L., Kohler, U. and Mantsch, H. H. (1988) Structural and conformational changes of β-lactoglobulin B: an infrared spectroscopic study of the effect of pH and temperature. Biochim. Biophys. Acta **957**, 11–20

21 Jackson, M. and Mantsch, H. H. (1992) Halogenated alcohols as solvent for proteins: FTIR spectroscopic studies. Biochim. Biophys. Acta **1118**, 139–143

22 Nicastro, G., de Chiara, C., Pedone, E., Tatò M., Rossi, M. and Bartolucci, S. (2000) NMR solution structure of a novel thioredoxin from *Bacillus acidocaldarius*. Possible determinants of protein stability. Eur. J. Biochem. **267**, 403–413

23 Krimm, S. and Bandekar, J. (1986) Vibrational spectroscopy and conformation of peptides, polypeptides and proteins. Adv. Protein Chem. **38**, 181–364

24 Chirgadze, Y. N., Fedorow, O. W. and Trushina, N. P. (1975) Estimation of amino acid residue side-chain absorption in the infrared spectra of protein solutions in heavy water. Biopolymers **14**, 679–694

25 Banecki, B., Zylicz, M., Bertoli, E. and Tanfani, F. (1992) Structural and functional relationships in Dnak and Dnak756 heat-shock proteins from *E. coli*. J. Biol. Chem. **267**, 25051–25058

26 Leonard, M. and Maentele, W. (1993) Fourier transform infrared spectroscopy and electrochemistry of the primary electron donor in *Rhodobacter sphaeroides and Rhodopseudomonas viridis* reaction center: vibrational modes of the pigments *in situ* and evidence for protein and water modes affected by P* formation. Biochemistry **32**, 4532–4538

27 Ptitsyn, O. B. (1992) The molten globule state. In Protein Folding (Creighton, T. E., ed.) pp. 243–300, W. H. Freeman and Company, New York

28 Filosa, A., Wang, Y., Ismail, A. A. and Englich, A. M. (2001) Two-domensional infrared correlation spectroscopy as a probe of sequential events in the thermal unfolding of cytochromes *c*. Biochemistry **40**, 8256–8263

29 Martin, J. L. (1995) Thioredoxin: a fold for all reasons. Structure (Cambridge, MA, U.S.A.) **3**, 245–250

30 Kennedy, D. F., Crisma, M., Toniolo, C. and Capman, D. (1991) Studies of peptides forming 310- and α-helices and β-bend ribbon structures in organic solutions and in model biomembranes by Furier transform infrared spectroscopy. Biochemistry **30**, 6541–6548

31 Soto, C. (2001) Protein misfolding and disease; protein refolding and therapy. FEBS Lett. **498**, 204–207

32 Jackson, M. and Mantsch, H. H. (1991) Beware of proteins in DMSO. Biochim. Biophys. Acta **1078**, 231–235

33 Bychkova, V. E., Dujsekina, A. E., Klenin, S. I., Tiktopulo, E. I., Uversky, V. N. and Ptitsyn, O. B. (1996) Molten globule-like state of cytochrome *c* under conditions simulating those near the membrane surface. Biochemistry **35**, 6058–6063

34 Bychkova, V. E., Pain, R. H. and Ptitsyn, O. B. (1988) The molten globule state is involved in the translocation of proteins across membranes? FEBS Lett. **238**, 231–234

35 Dolgikh, D. A., Gilmanshin, R. I., Brazhnikov, E. V., Bychkova, V. E., Semisotnov, G. V., Venyaminov, S.Yu. and Ptitsyn, O. B. (1981) α-Lactalbumin: compact state with fluctuating tertiary structure? FEBS Lett. **136**, 311–315

36 Dolgikh, D. A., Abaturov, L. V., Bolotina, I. A., Brazhnikov, E. V., Bushuev, V. N., Bychkova, V. E., Gilmanshin, R. I., Lebedev, Yu.O., Semisotnov, G. V., Tiktopulo, E. I. and Ptitsyn, O. B. (1985) Compact state of a protein molecule with pronounced small-scale mobility: bovine α-lactalbumin. Eur. Biophys. J. **13**, 109–121